HHS Public Access

Author manuscript

Dev Biol. Author manuscript; available in PMC 2024 November 01.

Published in final edited form as:

Dev Biol. 2023 November ; 503: 1–9. doi:10.1016/j.ydbio.2023.07.005.

Developmental origin of the mammalian premaxilla

Paul P. R. Iyyanar[1], **Chuanqi Qin**[1,2], **Nirpesh Adhikari**[1], **Han Liu**[1], **Yueh-Chiang Hu**[1,4], **Rulang Jiang**[1,3,4,*], **Yu Lan**[1,3,4,*]

[1]Division of Developmental Biology, Cincinnati Children's Hospital Medical Center, Cincinnati, Ohio, United States;

[2]The State Key Laboratory Breeding Base of Basic Science of Stomatology (Hubei-MOST) & Ministry of Education Key Laboratory of Oral Biomedicine, School & Hospital of Stomatology, Wuhan University, Wuhan, Hubei, China;

[3]Division of Plastic Surgery, Cincinnati Children's Hospital Medical Center, Cincinnati, Ohio, United States;

[4]Departments of Pediatrics and Surgery, University of Cincinnati College of Medicine, Cincinnati, Ohio, United States.

Abstract

The evolution of jaws has played a major role in the success of vertebrate expansion into a wide variety of ecological niches. A fundamental, yet unresolved, question in craniofacial biology is about the origin of the premaxilla, the most distal bone present in the upper jaw of all amniotes. Recent reports have suggested that the mammalian premaxilla is derived from embryonic maxillary prominences rather than the frontonasal ectomesenchyme as previously shown in studies of chicken embryos. However, whether mammalian embryonic frontonasal ectomesenchyme contributes to the premaxillary bone has not been investigated and a tool to trace the contributions of the frontonasal ectomesenchyme to facial structures in mammals is lacking. The expression of the *Alx3* gene is activated highly specifically in the frontonasal ectomesenchyme, but not in the maxillary mesenchyme, from the beginning of facial morphogenesis in mice. Here, we report the generation and characterization of a novel $Alx3^{CreERT2}$ knock-in mouse line that express tamoxifen-inducible Cre DNA recombinase from the *Alx3* locus. Tamoxifen treatment of $Alx3^{CreERT2/+};Rosa26^{mTmG/+}$ embryos at E7.5, E8.5, E9.5, and E10.5, each induced specific labeling of the embryonic medial nasal and lateral nasal mesenchyme but not the maxillary mesenchyme. Lineage tracing of $Alx3^{CreERT2}$-labeled frontonasal mesenchyme from E9.5 to E16.5 clearly showed that the frontonasal mesenchyme cells give rise to the osteoblasts generating

*Corresponding authors: Rulang.Jiang@CCHMC.org, Yu.Lan@cchmc.org.

Author Contributions

P.P.R. Iyyanar contributed to data acquisition and interpretation, drafted and critically revised the manuscript; C. Qin, N. Adhikari, and H. Liu contributed to data acquisition and revision of the manuscript; Y.-C. Hu contributed to design, data interpretation, and revision of the manuscript; R. Jiang contributed to conception, design, data acquisition and interpretation, drafted and critically revised the manuscript; Y. Lan contributed to design, data acquisition and interpretation, and critically revised the manuscript. All authors gave final approval and agree to be accountable for all aspects of the work.

the premaxillary bone. Furthermore, we characterize a *Dlx1-Cre* BAC transgenic mouse line that expresses Cre activity in the embryonic maxillary but not frontonasal mesenchyme and show that the *Dlx1-Cre* labeled embryonic maxillary mesenchyme cells contribute to the maxillary bone as well as the soft tissues lateral to both the premaxillary and maxillary bones but not to the premaxillary bone. These results clearly demonstrate the developmental origin of the premaxillary bone from embryonic frontonasal ectomesenchyme cells in mice and confirm the evolutionary homology of the premaxilla across amniotes.

Graphical Abstract

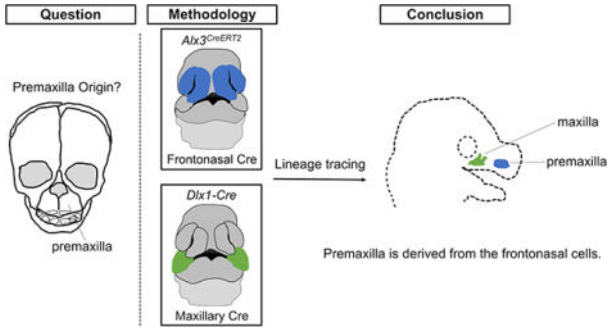

Keywords

craniofacial; frontonasal; lineage tracing; neural crest; Alx3; Dlx1

Introduction

Formation of jaws is a pivotal vertebrate innovation, which enabled early gnathostomes to become effective predators and expand into various new ecological niches (Kuratani, 2004, 2021; Mallatt, 2008). Subsequent evolution of the jaws and adaptations such as teeth and beaks facilitated more efficient and specialized feeding mechanisms, which ushered in enormous diversity not only in general body shape and size but also in jaw structures and function, as exemplified by the vast variety of amniote jaws (Abramyan and Richman, 2015; Davit-Beal et al., 2009; Richman et al., 2006; Woronowicz and Schneider, 2019). Whereas the jaws of a generalized amniote ancestor consist of the palatoquadrate cartilage in the upper jaw and Meckel's cartilage in the lower jaw, these cartilages are not major contributors to functional adult jaws in modern amniotes. Instead, the functional upper jaw of amniotes is made up of multiple dermal bones including the premaxilla, maxilla, quadratojugal, palatine, and pterygoid bones (Woronowicz and Schneider, 2019). Furthermore, the jaw bones in different taxa changed significantly in response to selective pressure during the course of evolution, resulting in major differences in their morphology, position, number, and function (Richman et al., 2006). For example, the septomaxilla, a pair of bones associated with the nasolacrimal duct and located between the premaxilla and nasal bones, is present in many primitive amniotes but is absent in birds and the majority of mammals with the exception of monotremes and edentates (Richman et al., 2006). In birds, the largest bone in the upper jaw is the palatine bone whereas the maxillary bones are very small and premaxillary bones are rostrally expanded and fused to form the upper beak (Bhullar et al., 2015; Richman et

al., 2006; Woronowicz and Schneider, 2019). In mammals, the maxillary bones comprise most of the upper jaw whereas the premaxilla is relatively small and recessed such that the nasal cavity is often projected outward beyond the premaxilla (Higashiyama et al., 2021; Higashiyama et al., 2023; Richman et al., 2006). The morphological diversity and lineage specific differences in topographical relationships of the jaw bones have made it difficult to determine homology among amniote facial bones and led to distinct hypotheses regarding the evolution of amniote jaws (Higashiyama et al., 2021; Higashiyama et al., 2023; Richman et al., 2006).

Despite major differences in postnatal jaw structures, all amniote facial bones are derived from cranial neural crest cells (CNCCs) that populate embryonic facial prominences around the primitive oral cavity, including the frontonasal prominence (FNP), paired maxillary processes (MxP) and mandibular processes (Abramyan and Richman, 2015; Richman et al., 2006). The FNP grows and expands around the bilateral nasal placodes to form the medial nasal processes (MNP) and lateral nasal processes (LNP) distally. Formation of the intact upper jaw involves convergence and fusion of MxP medially with LNP and MNP while the midline merging of MNP generates the primary palate (Abramyan and Richman, 2015; Jiang et al., 2006). Whereas the most commonly used animal models for craniofacial development studies are birds and mammals, particularly chicken and mouse, there are lineage-specific morphological variations during ontogeny of the amniote upper jaw (Abramyan and Richman, 2015; Richman et al., 2006). For example, a deep furrow forms at the embryonic facial midline dividing the MNP during early mouse facial morphogenesis whereas the chicken embryos develop a single midline structure, called the frontonasal mass, medial to the nasal pits (Abramyan and Richman, 2015). Nevertheless, it is clear from embryological studies that the frontonasal mass of chicken and reptilian embryos is homologous to mouse MNP (Abramyan and Richman, 2015). Whereas fate mapping and lineage tracing studies in chicken embryos showed that the frontonasal mass forms nasal cartilages and premaxillary bone while MxP forms maxillary and palatine as well as jugal bones (Cerny et al., 2004; Lee et al., 2004; Richman and Tickle, 1989, 1992; Wedden, 1987), a recent lineage tracing analysis using the *Dlx1*^{CreERT2} mouse line, which expresses tamoxifen-inducible Cre activity in embryonic maxillary and mandibular processes, led to the suggestion that MxP cells contributed to premaxillary bones in mice (Higashiyama et al., 2021). This finding and additional comparative analysis of synapid fossils led to the suggestion that the mammalian face is an evolutionary novelty with its premaxilla replaced by MxP derived septomaxilla (Higashiyama et al., 2021; Higashiyama et al., 2023). However, the *Dlx1*^{CreERT2} lineage labeling was detected in a small subset of cells in the premaxillary osteogenic region (Higashiyama et al., 2021) and no direct lineage tracing analysis of embryonic frontonasal ectomesenchyme in facial bone development in mammals has been reported. In fact, a tool that specifically labels the mouse embryonic frontonasal mesenchyme, but not MxP cells, is lacking.

The *Alx3* gene encodes a member of the conserved Aristaless homeobox family of transcription factors with important roles in vertebrate craniofacial development (Beverdam et al., 2001; Farlie et al., 2016; Meijlink et al., 1999; ten Berge et al., 1998). During mouse embryogenesis, *Alx3* mRNA expression is first detected in the CNCC-derived frontonasal mesenchyme at E9 and later in the distal mandibular arches in addition to MNP and LNP

between E10 and E11.0 (Beverdam et al., 2001; ten Berge et al., 1998). In this study, we generated *Alx3*^{CreERT2} knockin mice and performed genetic lineage tracing of embryonic frontonasal ectomesenchyme to better understand the embryonic origins of mammalian facial structures. In addition, we found that the *Dlx1-Cre* BAC transgenic mouse line generated by the Gene Expression Nervous System Atlas (GENSAT) Project (Gerfen et al., 2013; Gong et al., 2007) exhibited Cre activity in embryonic MxP. We compared the contributions of the *Alx3*^{CreERT2} and *Dlx1-Cre* lineage cells in mouse craniofacial development and demonstrate clearly that the mouse premaxillary bone tissues are derived from embryonic frontonasal mesenchyme.

Materials and Methods

Generation of *Alx3*^{CreERT2} mice

A chemically modified sgRNA targeting exon2 of the *Alx3* gene (target sequence 5' CTACCAGTGGATTGCCGAGG 3') was purchased from Integrated DNA Technologies (IDT, Coralville, IA). A donor DNA template containing the *P2A-CreERT2* cassette and flanking homology arms was synthesized by GeneUniversal Inc. (Newark, DE). A mixture of the sgRNA, CAS9 protein (IDT, Catlog #1081061), and donor plasmid DNA at the final concentrations of 50:100:100 ng/μl was injected into the cytoplasm of C57BL/6J mouse zygotes using a piezo-driven technique (Scott and Hu, 2019). Injected eggs were transferred into the oviductal ampulla of pseudopregnant CD1 female mice at ~25 eggs per recipient. Pups born were genotyped for the *Alx3*^{CreERT2} sequences using specific primers P8 (5'CGGAGACTGAAGCCTCAGTGCTC3') and Cre-AS1 (5'CTGGCGATCCCTGAACATGTC3'). Founder and G1 heterozygous mice were sequence verified. *Alx3*^{CreERT2} mice have been maintained in the C57BL/6J background.

All animal work procedures were performed following the recommendations in the Guide for Care and Use of Laboratory Animals by National Institute of Health and approved by Institutional Animal Care and Use Committee at Cincinnati Children's Hospital Medical Center. This study conformed with the updated ARRIVE 2.0 (Animal Research: Reporting of *In Vivo* Experiments) guidelines for preclinical animal studies.

Additional mouse strains

The *R26R*$^{lacz/lacZ}$ (Soriano, 1999), *R26*$^{Ai3\text{-}YFP}$ (Madisen et al., 2010), and *Rosa26*^{mTmG} (Muzumdar et al., 2007) mice were maintained by sibling intercrossing. The *Dlx1-Cre* BAC transgenic mice [*Tg(Dlx1-cre)RB27Gsat*, RRID: MMRRC_036076-UCD] were obtained from GENSAT (Gong et al., 2007; Kuerbitz et al., 2018).

X-gal staining, *in situ* hybridization, and immunofluorescent staining

At least three embryos of each genotype at each developmental stage are used for each experimental assay. X-gal staining of whole mount embryos and cryosections was performed as described previously (Nagy et al., 2007). For embryos at E15.5 or later, stained embryos were cleared using CUBIC-1 clearing agent at 37°C with mild shaking as described (Watanabe-Takano et al., 2021). Tissue-cleared embryos were incubated in Alizarin red in 2% KOH solution overnight at room temperature and cleared for 18–24 hours.

Whole mount *in situ* hybridization was performed as previously described (Iyyanar et al. 2022). Immunofluorescent staining for SP7 (1:800; Abcam ab22552), GFP (1:500; Aves GFP-1020) were carried out on cryosections of 10 μm thickness.

Results

Alx3 gene expression during mouse facial development

Previous reports suggest that *Alx3* expression is highly restricted to developing frontonasal tissues but absent from embryonic MxP (Beverdam et al., 2001; Lakhwani et al., 2010). To verify the patterns of *Alx3* expression during mouse facial development, we examined *Alx3* mRNA expression in E9.5 to E11.5 embryos by whole mount *in situ* hybridization analysis. At E9.5, *Alx3* mRNAs were expressed in the FNP, but not in MxP and mandibular processes (Figure 1A, B). At E10.5, when the FNP is divided into MNP and LNP, *Alx3* mRNAs were strongly expressed in the MNP and in the distal-most region of mandibular processes, with moderate levels in LNP (Figure 1C). *Alx3* mRNAs continued to be expressed in MNP, LNP, and distal mandibular tissues at E11.5 (Figure 1D). No *Alx3* mRNA expression was detected in the MxP from E9.5 to E11.5 (Figure 1A–D).

Alx3^{CreERT2} mice provide a unique tool for lineage tracing of embryonic origins of facial structures

We generated *Alx3*$^{CreERT2/+}$ mice using CRISPR/cas9-mediated genome editing (Figure 2A–C). *Alx3*$^{CreERT2/+}$ mice are indistinguishable morphologically from wildtype mice. Of 30 progenies from intercrossing male and female *Alx3*$^{CreERT2/+}$ mice, 6 were *Alx3*$^{CreERT2/CreERT2}$ homozygotes (20%) and they exhibited normal life span and fertility. This is consistent with previous report indicating that most *Alx3* gene-knockout mice do not have morphological abnormality (Beverdam et al., 2001; Lakhwani et al., 2010).

We crossed *Alx3*$^{CreERT2/+}$ males with *Rosa26*^{mTmG} female mice and treated pregnant females with tamoxifen (TAM) once on gestational days E6.5 to E10.5 followed by collecting embryos at E11.5 to analyze the patterns of inducible Cre activity. No GFP+ cells were detected at any stage in *Alx3*$^{CreERT2/+}$;*Rosa26*$^{mTmG/+}$ embryos without TAM treatment. Few GFP+ cells were detected, and they were restricted to the MNP in *Alx3*$^{CreERT2/+}$;*Rosa26*$^{mTmG/+}$ embryos following TAM at E6.5. Treatment at E7.5, E8.5, E9.5, each resulted in consistent patterns of GFP+ cells in E11.5 *Alx3*$^{CreERT2/+}$;*Rosa26*$^{mTmG/+}$ embryos, with progressively increased proportion of GFP+ cells in the MNP and LNP with later TAM treatment (Figure 2D–G). This is consistent with recent scRNA-seq analyses that showed that *Alx3* expression was not activated in mouse CNCCs until E8.75 (Iyyanar et al., 2022; Zalc et al., 2021). In addition to MNP and LNP, GFP+ cells were detected in the distal mandible in E11.5 *Alx3*$^{CreERT2/+}$;*Rosa26*$^{mTmG/+}$ embryos following TAM treatment at E9.5 or E10.5 (Figure 2F, G), which is also consistent with the onset of *Alx3* mRNA expression in distal mandibular arches after E9.5 (Figure 1A–C).

To examine the patterns of Cre activity in *Alx3*$^{CreERT2/+}$ mice in more detail, we crossed *R26R*^{lacZ} reporter mice (Soriano, 1999) to *Alx3*$^{CreERT2/+}$ male mice and serially sectioned

E11.5 *Alx3*$^{CreERT2/+}$;*R26R*$^{lacz/+}$ embryos after TAM treatment at E9.5 (Figure 3A). X-gal staining of serial coronal sections showed a dynamic pattern of β-galactosidase (β-gal) activity in the craniofacial tissues. Sections through posterior region of developing eyes showed limited β-gal activity in the midline mesenchyme ventral to the diencephalon and extending laterally towards the eyes (Figure 3B). More anteriorly, strong β-gal activity was detected in periocular mesenchyme as well as throughout the frontonasal mesenchyme posterior to the primitive nasal cavity and between developing eyes (Figure 3C–E). On sections through the posterior end of the primitive nasal cavity, strong β-gal activity was observed throughout the MNP mesenchyme and in most of the LNP mesenchyme cells (Figure 3F). Sections through the middle of the primitive nasal cavity, where the primary choanae had formed from rupturing of the bucconasal membrane between LNP and MNP, showed β-gal activity throughout MNP mesenchyme but many LNP cells were not stained (Figure 3G). Further anterior sections showed strong β-gal activity in the MNP but significantly reduced labeling of LNP cells (Figure 3H, I). In addition, β-gal staining was detected in the midline region of distal mandible (Figure 3D–H) as well as in the mesenchyme between cerebral hemispheres (Figure 3H). Importantly, no *Cre* activity was detected in the maxillary prominence along the entire anterior-posterior axis. Thus, the *Alx3*$^{CreERT2/+}$ mice provide an unprecedented opportunity to examine the contributions of the embryonic frontonasal mesenchyme to facial structures.

Alx3^{CreERT2} lineage labeling clearly shows frontonasal mesenchyme contribution to the premaxillary bone

To investigate the contribution of *Alx3*^{CreERT2} expressing embryonic frontonasal mesenchyme cells to facial structures, we treated *Alx3*$^{CreERT2/+}$;*R26R*$^{lacz/+}$ embryos with TAM at E9.5 and E10.5, respectively, and visualized β-gal activity at E15.5 to E16.5. Strong β-gal activity was detected in the premaxilla in addition to the nasal capsule and distal part of the tongue and mandible in E15.5 *Alx3*$^{CreERT2/+}$;*R26R*$^{lacz/+}$ embryos following TAM treatment at either E9.5 or E10.5 (Figure 4A–F). Co-staining with Alizarin red showed robust β-gal activity in the premaxillary bone tissues while maxillary bone remained negative of β-gal staining in E15.5 *Alx3*$^{CreERT2/+}$;*R26R*$^{lacz/+}$ embryos (Figure 4C, F). Serial transverse sections of E16.5 *Alx3*$^{CreERT2/+}$;*R26R*$^{lacz/+}$ embryo heads following TAM treatment at E10.5 clearly showed restricted patterns of β-gal activity in nasal capsule and the premaxillary bone tissues surrounding the developing upper incisor but complete absence of β-gal activity in maxillary bone (Figure 4G–I). Furthermore, co-immunostaining for the osteoblast marker SP7 and Cre-activated YFP in transverse sections of E15.5 *Alx3*$^{CreERT2/+}$;*Rosa26*$^{Ai3\text{-}YFP/+}$ embryos following TAM at E9.5 showed colocalization of SP7 and YFP throughout the premaxillary osteogenic tissues but absence of YFP in the SP7-positive maxillary osteogenic tissues (Figure 4J–L). Together, these data indicate that the embryonic frontonasal mesenchyme cells make a major contribution to the premaxillary bone in mice.

Analysis of Dlx1-Cre BAC transgenic mice and comparative analysis of contributions of Dlx1-Cre and Alx3^{CreERT2} lineage cells to the upper jaw

Higashiyama et al. reported contribution of *Dlx1*^{CreERT2} marked embryonic cells to the premaxillary bone in *Dlx1*$^{CreERT2/+}$;*R26R*$^{lacz/+}$ and *Dlx1*$^{CreERT2/+}$;*R26R*$^{YFP/+}$ embryos

following TAM treatment at E10.5 (Higashiyama et al., 2021). Since we could not obtain the *Dlx1*$^{CreERT2/+}$ mice for comparative studies, we examined Cre activity in the *Dlx1-Cre* BAC transgenic mice (Kuerbitz et al., 2018), which carry a transgene containing 185-kb of genomic DNA surrounding the *Dlx1* locus in which a Cre expression cassette was inserted at the *Dlx1* translation initiation codon. Consistent with the patterns of X-gal staining reported in *Dlx1*$^{CreERT2/+}$;*R26R*$^{lacz/+}$ mouse embryos (Higashiyama et al., 2021), *Dlx1-Cre*;*R26R*$^{lacz/+}$ embryos displayed strong β-gal activity in MxP and proximal mandibular processes at E10.5 (Figure 5A). *Dlx1-Cre*;*R26R*$^{lacz/+}$ embryos also displayed β-gal activity in a subset of nasal pit epithelial cells but not in MNP and LNP mesenchyme cells (Figure 5A). Whole mount E15.5 *Dlx1-Cre*; *R26R*$^{lacz/+}$ embryos showed strong β-gal activity in maxillary tissues up to the distal tip of the upper jaw, but the frontonasal and primary palate tissues appeared mostly negative (Figure 5B, C). To examine contributions of *Dlx1-Cre* labeled cells in detail, we serially sectioned E15.5 *Dlx1-Cre;R26R*$^{lacz/+}$ embryo heads in the transverse plane and performed X-gal staining of the cryosections. Whereas β-gal labeling was evident in developing maxillary bone as well as in soft tissues lateral to both premaxillary and maxillary bones, cells in the developing premaxillary bone surrounding the upper incisor, except the dental follicle cells immediately adjacent to the incisor tooth germ, remained largely unlabeled in *Dlx1-Cre;R26R*$^{lacz/+}$ embryos (Figure 5D–G).

To clarify contributions of *Dlx1-Cre* and *Alx3*^{CreERT2} labelled cells, respectively, to the upper jaw, we compared patterns of X-gal staining of serial frontal sections of E15.5 *Dlx1-Cre*;*R26R*$^{lacz/+}$ embryos with those of E15.5 *Alx3*$^{CreERT2/+}$;*R26R*$^{lacz/+}$ embryos treated with TAM at E10.5 (Figure 6). The patterns of β-gal staining clearly showed that *Dlx1-Cre* labeled cells contributed to the maxillary bone and the soft tissues lateral to both premaxillary and maxillary bones, but not to the premaxillary bone tissues except the incisor dental follicle cells, whereas *Alx3*^{CreERT2} labeled cells contributed to nasal cartilages, nasal bone, and premaxillary bone tissues surrounding the upper incisor (Figure 6). To better visualize the contributions of *Alx3*^{CreERT2} labelled frontonasal mesenchyme versus that of the *Dlx1-Cre* labeled embryonic maxillary mesenchyme around the premaxillary-maxillary boundary regions, we performed X-gal staining of serial parasagittal sections of the E16.5 *Dlx1-Cre*;*R26R*$^{lacz/+}$ embryos and E16.5 *Alx3*$^{CreERT2/+}$;*R26R*$^{lacz/+}$ embryos treated with TAM at E9.5. Images of the X-gal staining patterns from representative serial sections from the buccal side to the lingual side, each cutting through the premaxillary-maxillary boundary region, are shown in Fig. 7. These data clearly show *Dlx1-Cre* lineage cells throughout the maxillary tissues including the ossifying maxillary tissue and the molar tooth mesenchyme, but no *Dlx1-Cre* lineage cells in the ossifying premaxillary tissue except in a few dental follicle cells at the base of the upper incisor (Fig. 7A–F). On the other hand, the *Alx3*^{CreERT2} lineage labeled cells were found throughout the incisor tooth mesenchyme and the ossifying premaxillary tissue but no *Alx3*^{CreERT2} lineage cells were detected in the maxillary bone tissue (Fig. 7G–L). Together, these data clearly demonstrate that the mouse premaxillary bone, including lateral aspect of the incisive bone, is derived from the embryonic frontonasal mesenchyme whereas the embryonic MxP gives rise to the maxillary bones and upper jaw soft tissues, including the soft tissues lateral to the premaxillary bone.

Discussion

The premaxillary bone is present and located most distally in the upper jaw of all amniotes examined (Abramyan and Richman, 2015; Richman et al., 2006). While it is widely accepted that the premaxillary bone is homologous across amniotes and is derived from CNCCs, the embryonic origins of the premaxillary and maxillary bones and their relationship with facial prominences have only been systematically studied in chicken embryos (Richman et al., 2006; Santagati and Rijli, 2003). Fate mapping and lineage tracing studies in chicken embryos showed that frontonasal mesenchyme cells give rise to the premaxilla, nasal cartilage, and frontal bone, whereas the MxP cells contribute to maxillary, palatine, jugal, and quadratojugal bones but not the premaxilla (Cerny et al., 2004; Lee et al., 2004; Richman and Tickle, 1989, 1992; Wedden, 1987). Higashiyama et al. recently studied embryonic origins of mouse facial bones using the *Dlx1*^{CreERT2} mice and found that *Dlx1*^{CreERT2} lineage labelled cells not only contributed to maxillary and mandibular bones but also the premaxilla (Higashiyama et al., 2021). Despite only a small subset of cells in the Runx2+ premaxillary osteogenic region were shown positive for the lineage marker, they concluded that the therian premaxilla is predominantly of the maxillary prominence origin (Higashiyama et al., 2021). In this study, we generated *Alx3*^{CreERT2} knockin mice that enabled Cre/loxP-mediated lineage tracing specifically of frontonasal ectomesenchyme. Our data demonstrate that the mouse premaxillary bone is predominantly, if not exclusively, derived from frontonasal ectomesenchyme. Furthermore, we performed lineage tracing using *Dlx1-Cre* BAC transgenic mice, which exhibits strong constitutive Cre activity in the embryonic maxillary mesenchyme, and found that the *Dlx1-Cre* lineage cells contributed to maxillary bone as well as soft tissues lateral to both maxillary and premaxillary ossification centers but not in the osteogenic cells of the premaxilla. We did detect strong *Dlx1-Cre* activated lineage marker in the dental follicle cells immediately adjacent to the upper incisor tooth germs surrounded by unlabeled premaxillary osteogenic cells. It is likely that labeling of incisor dental follicle cells reflected specific *Dlx1-Cre* expression in those cells, but they are not descendants of the MxP mesenchyme. Altogether, our results indicate that the mouse premaxilla is indeed homologous to chicken premaxilla with regards to their ontogeny.

Higashiyama et al. suggested that the mammalian-specific face, the muzzle, is an evolutionary novelty with a novel topological framework of the craniofacial mesenchyme compared with other vertebrates (Higashiyama et al., 2021). We found that the *Dlx1-Cre* lineage cells contribute to much of the soft tissues covering both the maxillary and premaxillary bones, reaching to the anterior tip of the upper jaw, whereas *Alx3*^{CreERT2} labeled frontonasal mesenchyme cells contribute to the philtrum and primary palate in addition to the premaxillary bone and nasal tissues. Thus, while our data clearly show that the premaxillary bone is derived from the frontonasal mesenchyme rather than from the embryonic maxillary mesenchyme as suggested by Higashiyama et al. (Higashiyama et al., 2021; Higashiyama et al., 2023), our data do support the idea that morphogenesis of the therian face involves novel topological rearrangements of the craniofacial mesenchyme of embryonic frontonasal and maxillary processes, which results in the maxillary process-derived soft tissues reaching to the distal tip of the upper jaw and covering the frontonasal mesenchyme-derived premaxillary bone. The *Alx3*^{CreERT2} mice provide a unique tool to

genetically dissect the cellular and molecular mechanisms regulating morphogenesis of the mammalian face.

Mutations in *ALX3* cause frontonasal dysplasia type I in human (Twigg et al., 2009). In addition to being an *Alx3* mutant mouse line for studies of ALX family gene function in organogenesis and pathogenic mechanisms of frontonasal dysplasia, the $Alx3^{CreERT2/+}$ mice provide a valuable tool for both genetic lineage tracing of specific subset of CNCCs and for Cre/loxP mediated conditional genetic studies of cellular and molecular mechanisms of mammalian development. We demonstrate using Cre/loxP mediated genetic lineage tracing that the mouse premaxillary bone is derived from the CNCC-derived frontonasal mesenchyme, not the maxillary mesenchyme as recently reported (Higashiyama et al., 2021; Higashiyama et al., 2023). The $Alx3^{CreERT2}$ mice also enable inducible Cre-loxP mediated gene loss and/or gain of function studies related to craniofacial anomalies and will be particularly informative for delineating gene function and developmental mechanisms underlying cleft lip/palate pathogenesis. Furthermore, *Alx3* is expressed in several other tissues including periocular mesenchyme surrounding the developing eye, a subset of cells in the developing limb, body wall, urethra, and in pancreatic islet cells (Mirasierra and Vallejo, 2006; ten Berge et al., 1998). Thus, the $Alx3Cre^{ERT2}$ mice will be a valuable tool for studies of many developmental and disease processes. We will deposit the $Alx3^{CreERT2/+}$ mouse line to a publicly accessible Mutant Mouse Research and Resource Center for distribution to the research community.

Acknowledgements

We thank Cincinnati Children's Hospital Medical Center Transgenic Animal and Genome Editing Core facility for help with the generation of the $Alx3^{CreERT2}$ mice. We thank Kenny Campbell for sharing the *Dlx1-Cre* BAC transgenic mice. We thank Lindsey Barske for discussions. This work was supported by the National Institutes of Health/National Institute of Dental and Craniofacial Research (NIH/NIDCR) (grant number R01DE029417). The authors declare no conflict of interest with respect to the authorship and/or publication of this article.

References

Abramyan J, Richman JM, 2015. Recent insights into the morphological diversity in the amniote primary and secondary palates. Dev Dyn 244, 1457–1468. [PubMed: 26293818]

Beverdam A, Brouwer A, Reijnen M, Korving J, Meijlink F, 2001. Severe nasal clefting and abnormal embryonic apoptosis in Alx3/Alx4 double mutant mice. Development 128, 3975–3986. [PubMed: 11641221]

Bhullar BA, Morris ZS, Sefton EM, Tok A, Tokita M, Namkoong B, Camacho J, Burnham DA, Abzhanov A, 2015. A molecular mechanism for the origin of a key evolutionary innovation, the bird beak and palate, revealed by an integrative approach to major transitions in vertebrate history. Evolution 69, 1665–1677. [PubMed: 25964090]

Cerny R, Lwigale P, Ericsson R, Meulemans D, Epperlein HH, Bronner-Fraser M, 2004. Developmental origins and evolution of jaws: new interpretation of "maxillary" and "mandibular". Dev Biol 276, 225–236. [PubMed: 15531376]

Davit-Beal T, Tucker AS, Sire JY, 2009. Loss of teeth and enamel in tetrapods: fossil record, genetic data and morphological adaptations. J Anat 214, 477–501. [PubMed: 19422426]

Farlie PG, Baker NL, Yap P, Tan TY, 2016. Frontonasal Dysplasia: Towards an Understanding of Molecular and Developmental Aetiology. Mol Syndromol 7, 312–321. [PubMed: 27920634]

Gerfen CR, Paletzki R, Heintz N, 2013. GENSAT BAC cre-recombinase driver lines to study the functional organization of cerebral cortical and basal ganglia circuits. Neuron 80, 1368–1383. [PubMed: 24360541]

Gong S, Doughty M, Harbaugh CR, Cummins A, Hatten ME, Heintz N, Gerfen CR, 2007. Targeting Cre recombinase to specific neuron populations with bacterial artificial chromosome constructs. J Neurosci 27, 9817–9823. [PubMed: 17855595]

Higashiyama H, Koyabu D, Hirasawa T, Werneburg I, Kuratani S, Kurihara H, 2021. Mammalian face as an evolutionary novelty. Proc Natl Acad Sci U S A 118.

Higashiyama H, Koyabu D, Kurihara H, 2023. Evolution of the therian face through complete loss of the premaxilla. Evol Dev 25, 103–118. [PubMed: 36017615]

Iyyanar PPR, Wu Z, Lan Y, Hu YC, Jiang R, 2022. Alx1 Deficient Mice Recapitulate Craniofacial Phenotype and Reveal Developmental Basis of ALX1-Related Frontonasal Dysplasia. Front Cell Dev Biol 10, 777887. [PubMed: 35127681]

Jiang R, Bush JO, Lidral AC, 2006. Development of the upper lip: morphogenetic and molecular mechanisms. Dev Dyn 235, 1152–1166. [PubMed: 16292776]

Kuerbitz J, Arnett M, Ehrman S, Williams MT, Vorhees CV, Fisher SE, Garratt AN, Muglia LJ, Waclaw RR, Campbell K, 2018. Loss of Intercalated Cells (ITCs) in the Mouse Amygdala of Tshz1 Mutants Correlates with Fear, Depression, and Social Interaction Phenotypes. J Neurosci 38, 1160–1177. [PubMed: 29255003]

Kuratani S, 2004. Evolution of the vertebrate jaw: comparative embryology and molecular developmental biology reveal the factors behind evolutionary novelty. J Anat 205, 335–347. [PubMed: 15575882]

Kuratani S, 2021. Evo-devo studies of cyclostomes and the origin and evolution of jawed vertebrates. Curr Top Dev Biol 141, 207–239. [PubMed: 33602489]

Lakhwani S, García-Sanz P, Vallejo M, 2010. Alx3-deficient mice exhibit folic acid-resistant craniofacial midline and neural tube closure defects. Dev Biol 344, 869–880. [PubMed: 20534379]

Lee SH, Bedard O, Buchtova M, Fu K, Richman JM, 2004. A new origin for the maxillary jaw. Dev Biol 276, 207–224. [PubMed: 15531375]

Madisen L, Zwingman TA, Sunkin SM, Oh SW, Zariwala HA, Gu H, Ng LL, Palmiter RD, Hawrylycz MJ, Jones AR, Lein ES, Zeng H, 2010. A robust and high-throughput Cre reporting and characterization system for the whole mouse brain. Nat Neurosci 13, 133–140. [PubMed: 20023653]

Mallatt J, 2008. The origin of the vertebrate jaw: neoclassical ideas versus newer, development-based ideas. Zoolog Sci 25, 990–998. [PubMed: 19267635]

Meijlink F, Beverdam A, Brouwer A, Oosterveen TC, Berge DT, 1999. Vertebrate aristaless-related genes. Int J Dev Biol 43, 651–663. [PubMed: 10668975]

Mirasierra M, Vallejo M, 2006. The homeoprotein Alx3 expressed in pancreatic beta-cells regulates insulin gene transcription by interacting with the basic helix-loop-helix protein E47. Mol Endocrinol 20, 2876–2889. [PubMed: 16825292]

Muzumdar MD, Tasic B, Miyamichi K, Li L, Luo L, 2007. A global double-fluorescent Cre reporter mouse. Genesis 45, 593–605. [PubMed: 17868096]

Nagy A, Gertsenstein M, Vintersten K, Behringer R, 2007. Staining Whole Mouse Embryos for beta-Galactosidase (lacZ) Activity. CSH Protoc 2007, pdb prot4725.

Richman JM, Buchtova M, Boughner JC, 2006. Comparative ontogeny and phylogeny of the upper jaw skeleton in amniotes. Dev Dyn 235, 1230–1243. [PubMed: 16496291]

Richman JM, Tickle C, 1989. Epithelia are interchangeable between facial primordia of chick embryos and morphogenesis is controlled by the mesenchyme. Dev Biol 136, 201–210. [PubMed: 2806720]

Richman JM, Tickle C, 1992. Epithelial-mesenchymal interactions in the outgrowth of limb buds and facial primordia in chick embryos. Dev Biol 154, 299–308. [PubMed: 1426640]

Santagati F, Rijli FM, 2003. Cranial neural crest and the building of the vertebrate head. Nat Rev Neurosci 4, 806–818. [PubMed: 14523380]

Scott MA, Hu YC, 2019. Generation of CRISPR-Edited Rodents Using a Piezo-Driven Zygote Injection Technique. Methods Mol Biol 1874, 169–178. [PubMed: 30353513]

Soriano P, 1999. Generalized lacZ expression with the ROSA26 Cre reporter strain. Nat Genet 21, 70–71. [PubMed: 9916792]

ten Berge D, Brouwer A, el Bahi S, Guénet JL, Robert B, Meijlink F, 1998. Mouse Alx3: an aristaless-like homeobox gene expressed during embryogenesis in ectomesenchyme and lateral plate mesoderm. Dev Biol 199, 11–25. [PubMed: 9676189]

Twigg SR, Versnel SL, Nürnberg G, Lees MM, Bhat M, Hammond P, Hennekam RC, Hoogeboom AJ, Hurst JA, Johnson D, Robinson AA, Scambler PJ, Gerrelli D, Nürnberg P, Mathijssen IM, Wilkie AO, 2009. Frontorhiny, a distinctive presentation of frontonasal dysplasia caused by recessive mutations in the ALX3 homeobox gene. Am J Hum Genet 84, 698–705. [PubMed: 19409524]

Watanabe-Takano H, Ochi H, Chiba A, Matsuo A, Kanai Y, Fukuhara S, Ito N, Sako K, Miyazaki T, Tainaka K, Harada I, Sato S, Sawada Y, Minamino N, Takeda S, Ueda HR, Yasoda A, Mochizuki N, 2021. Mechanical load regulates bone growth via periosteal Osteocrin. Cell Rep 36, 109380. [PubMed: 34260913]

Wedden SE, 1987. Epithelial-mesenchymal interactions in the development of chick facial primordia and the target of retinoid action. Development 99, 341–351. [PubMed: 3653006]

Woronowicz KC, Schneider RA, 2019. Molecular and cellular mechanisms underlying the evolution of form and function in the amniote jaw. Evodevo 10, 17. [PubMed: 31417668]

Zalc A, Sinha R, Gulati GS, Wesche DJ, Daszczuk P, Swigut T, Weissman IL, Wysocka J, 2021. Reactivation of the pluripotency program precedes formation of the cranial neural crest. Science 371.

Highlights

- Embryonic origin of mammalian premaxilla is controversial and not well studied.
- *Alx3*^{CreERT2} mice enable specific genetic analysis of frontonasal development.
- Lineage tracing shows frontonasal mesenchyme gives rise to mouse premaxillary bone.
- Results reject recently proposed unique embryonic origin of mammalian premaxilla.
- This paper clarifies embryonic origins and homology of mammalian facial bones.

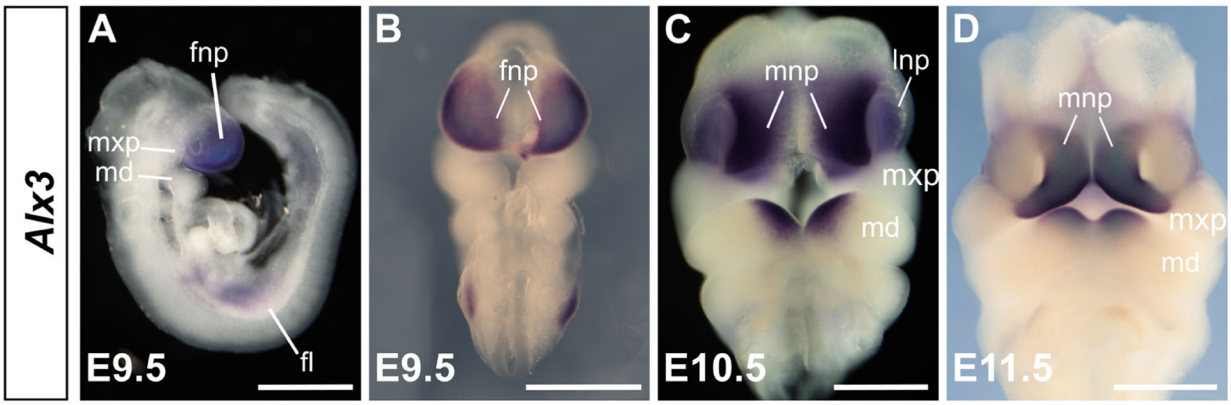

Figure 1. Expression of *Alx3* in craniofacial regions during embryonic development.

(A-D) Representative lateral (A) and frontal (B, C, D) views showing patterns of *Alx3* mRNA expression during craniofacial development at E9.5 (A and B) (n=4), E10.5 (C) (n=3), and E11.5 (D) (n=4). Scale bars in A-C are 500 μm and D,1000 μm, respectively. fl, forelimb; fnp, frontonasal prominence; lnp, lateral nasal process; md, mandible; mnp, medial nasal process; mxp, maxillary process.

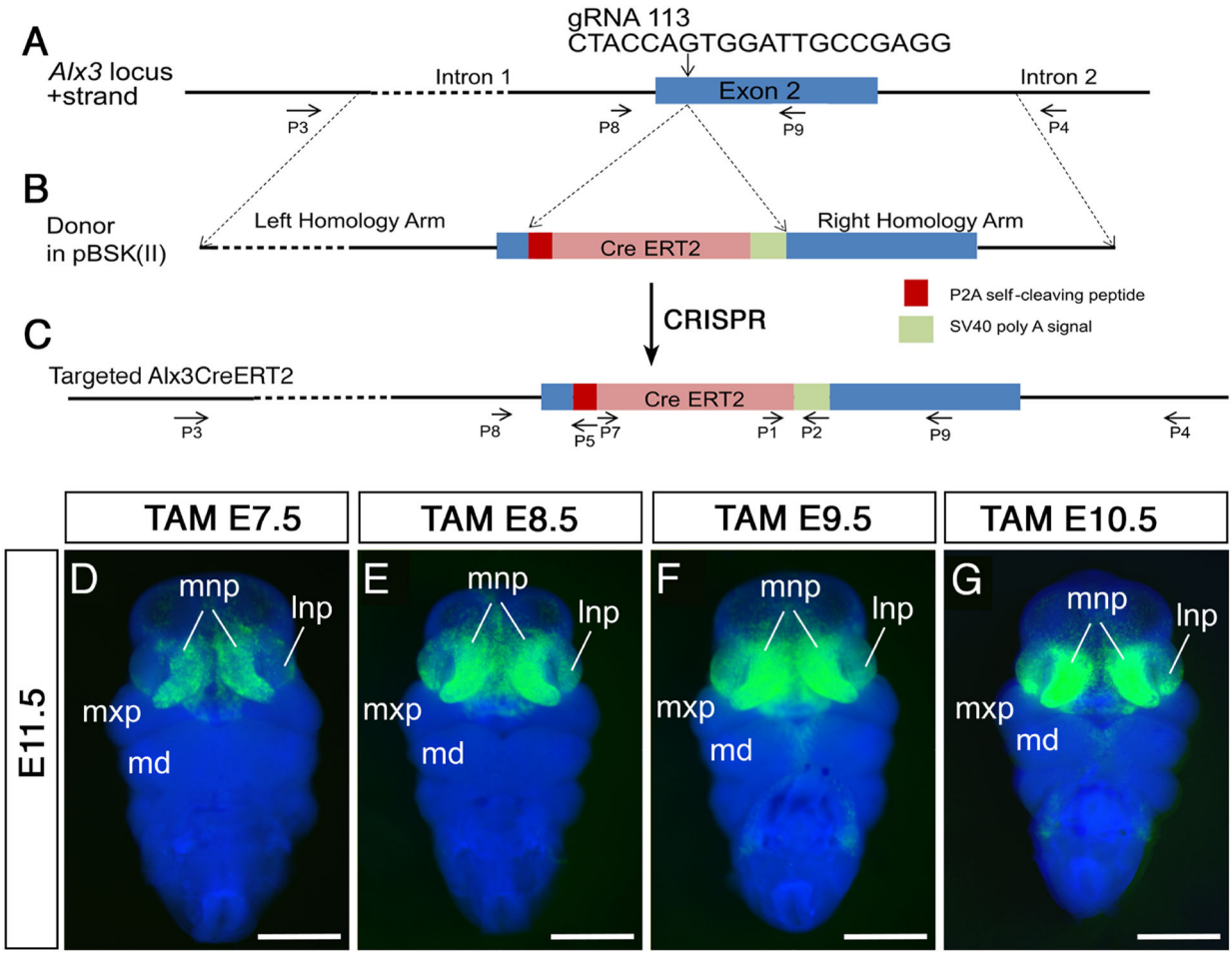

Figure 2. Strategy for generation of *Alx3*^{CreERT2} mice using CRISPR/CAS9 mediated genome editing and analysis of inducible Cre recombinase activity in *Alx3*^{CreERT2} mice.

(A-C) Schematic of CRISPR/CAS-9 mediated gene targeting strategy to insert the P2A-Cre-ERT2 sequences into exon-2 of the *Alx3* gene in Chromosome 3 (A, B) and the targeted *Alx3*$^{Cre\text{-}ERT2}$ allele (C). (D-G) Representative frontal views of *Alx3*$^{CreERT2/+}$;*Rosa26*$^{mTmG/+}$ embryo heads showing GFP fluorescence (green) after TAM treatment at E7.5 (A) (n=4), E8.5 (B) (n=5), E9.5 (C) (n=6), and E10.5 (D) (n=4). The non-recombined tdTomato is pseudo-colored in blue. Scale bars in A-D are 1000 μm. lnp, lateral nasal process; md, mandible; mnp, medial nasal process; mxp, maxillary process.

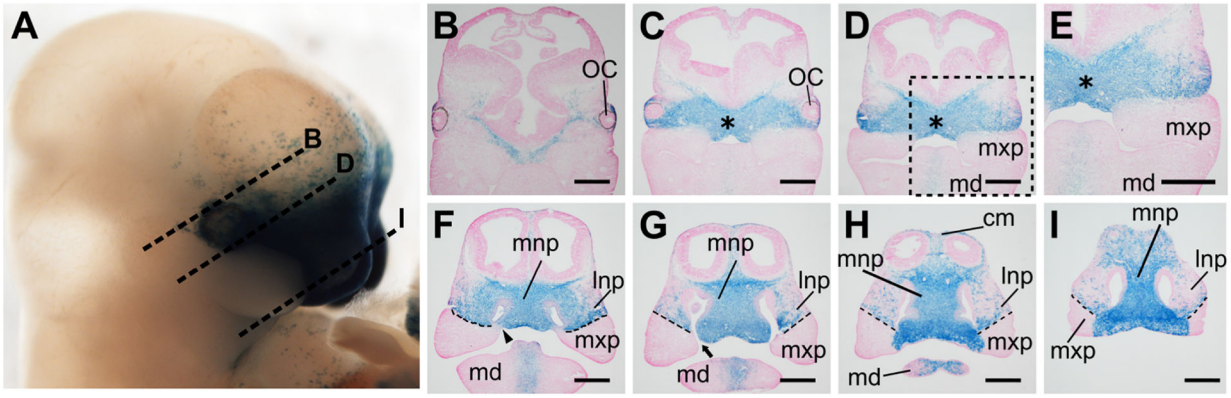

Figure 3. Patterns of β-galactosidase expression in the E11.5 *Alx3*^{CreERT2};*R26R*$^{lacz/+}$ embryos following TAM treatment at E9.5.

(A) A representative whole mouse X-gal stained E11.5 *Alx3*$^{CreERT2/+}$;*R26R*$^{lacz/+}$ embryo head (n=4), with representative planes of sections for images shown in B-I marked in dashed lines. (B-I) Serial frontal sections of an E11.5 *Alx3*$^{CreERT2/+}$;*R26R*$^{lacz/+}$ head through the eye (B-D) and frontonasal (F-I) regions. Higher magnification view of the boxed region in the panel D is shown in E. Scale bars, 500 μm. Asterisks in C-E point to the frontonasal ectomesenchyme cells in the posterior part of the frontonasal prominence. Arrowhead in F points to the site of fusion between the medial and lateral nasal processes near the posterior end of the primitive nasal cavity. Arrow in G points to the choana. cm, cranial mesenchyme; md, mandible; mnp, medial nasal process; lnp, lateral nasal process; mxp, maxillary process; oc, optic cup.

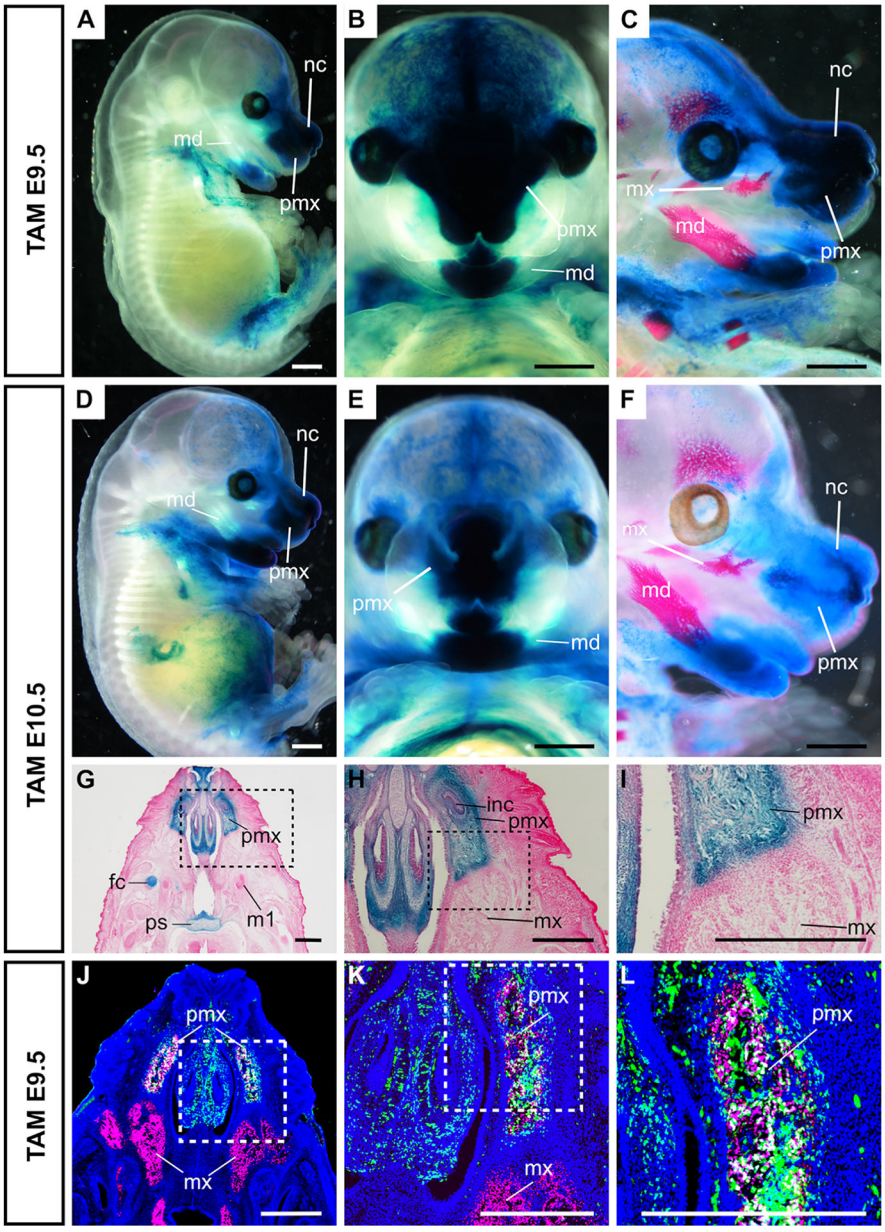

Figure 4. Lineage tracing of contribution of the *Alx3*^{CreERT2} labelled embryonic frontonasal ectomesenchyme cells to facial structures in E15.5 embryos.

(A-F) Whole mount views of β-gal reporter activity (blue color) in E15.5 *Alx3*$^{CreERT2/+}$;*R26R*$^{lacz/+}$ embryos following TAM treatment at E9.5 (A-C) (n=6) and E10.5 (D-F) (n=5), respectively. Developing bones in C and F were stained red using Alizarin red. (G-I) β-gal reporter activity (blue color) in the cryosections of E16.5 *Alx3*$^{CreERT2/+}$;*R26R*$^{lacz/+}$ embryos following TAM treatment at E10.5 (n=4). (J-L) Double immunofluorescence detection for SP7 (magenta) and YFP (green) in transverse sections of E15.5 *Alx3*$^{CreERT2/+}$;*Rosa*$^{Ai3\text{-}YFP/+}$ embryos after TAM treatment at E9.5 (n=4). Higher magnification views of boxed regions in panels G, H, J, and K are shown in H, I, K, and L, respectively. Scale bars in A-F are 1000 μm. Scale bars in G-L are 500 μm. fc, frontal

cartilage; inc, incisor; nc, nasal capsule; m1, first molar tooth, md, mandible; mx, maxillary bone; pmx, premaxillary bone, ps, presphenoid.

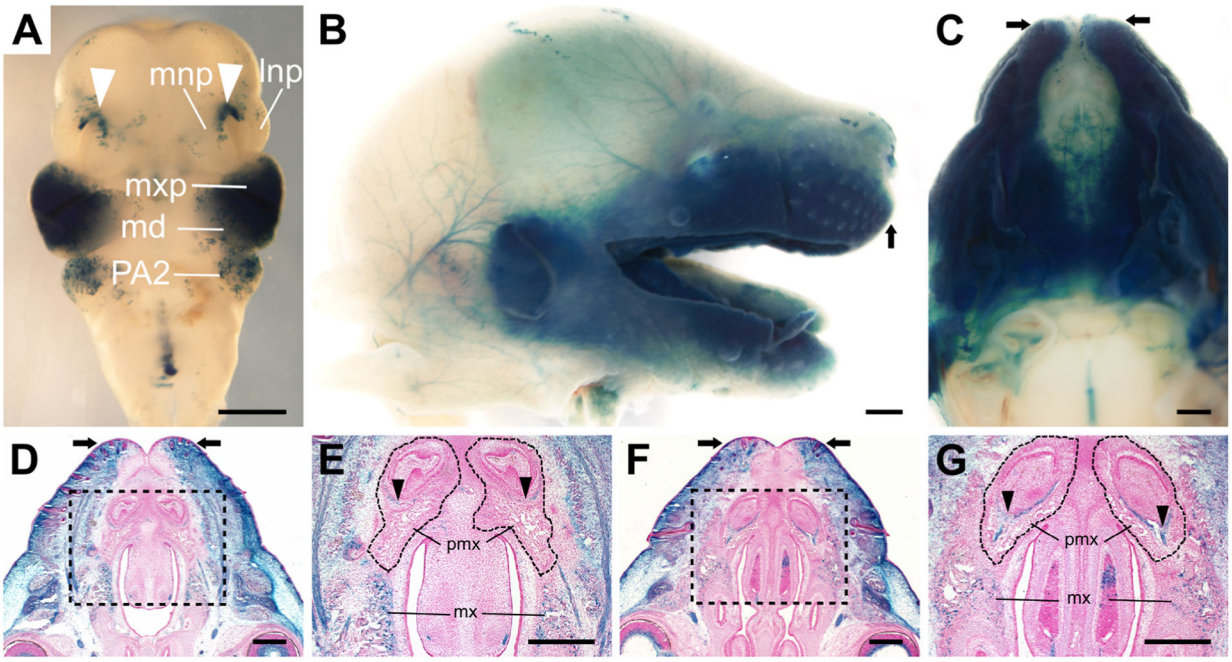

Figure 5. Patterns of β-gal reporter activity in *Dlx1-Cre;R26R*$^{lacz/+}$ embryos.

(A-C) Representative frontal (A), lateral (B) and palatal (C) views of *Dlx1-Cre;R26R*$^{lacz/+}$ embryo heads at E10.5 (A) (n=5) and E15.5 (B and C) (n=4). (D-G) Representative transverse sections of E15.5 *Dlx1-Cre;R26R*$^{lacz/+}$ embryo heads (n=4) through the developing maxillary and premaxillary bones. Higher magnification views of boxed regions in Panels D and F are shown in E and G, respectively. The premaxillary bone tissues in E and G are marked by black dashed outlines. White arrowheads in A point to the Cre activity in the nasal pit epithelia. Arrows in B, C, D, F point to the distal tip of the upper jaw. Black arrowheads in E and G point to the dental follicle cells associated with the upper incisor tooth germ. Scale bars 500 μm. lnp, lateral nasal process; md, mandible, mnp, medial nasal process; mx, maxillary bone; mxp, maxillary process; PA2, second pharyngeal arch; pmx, premaxillary bone.

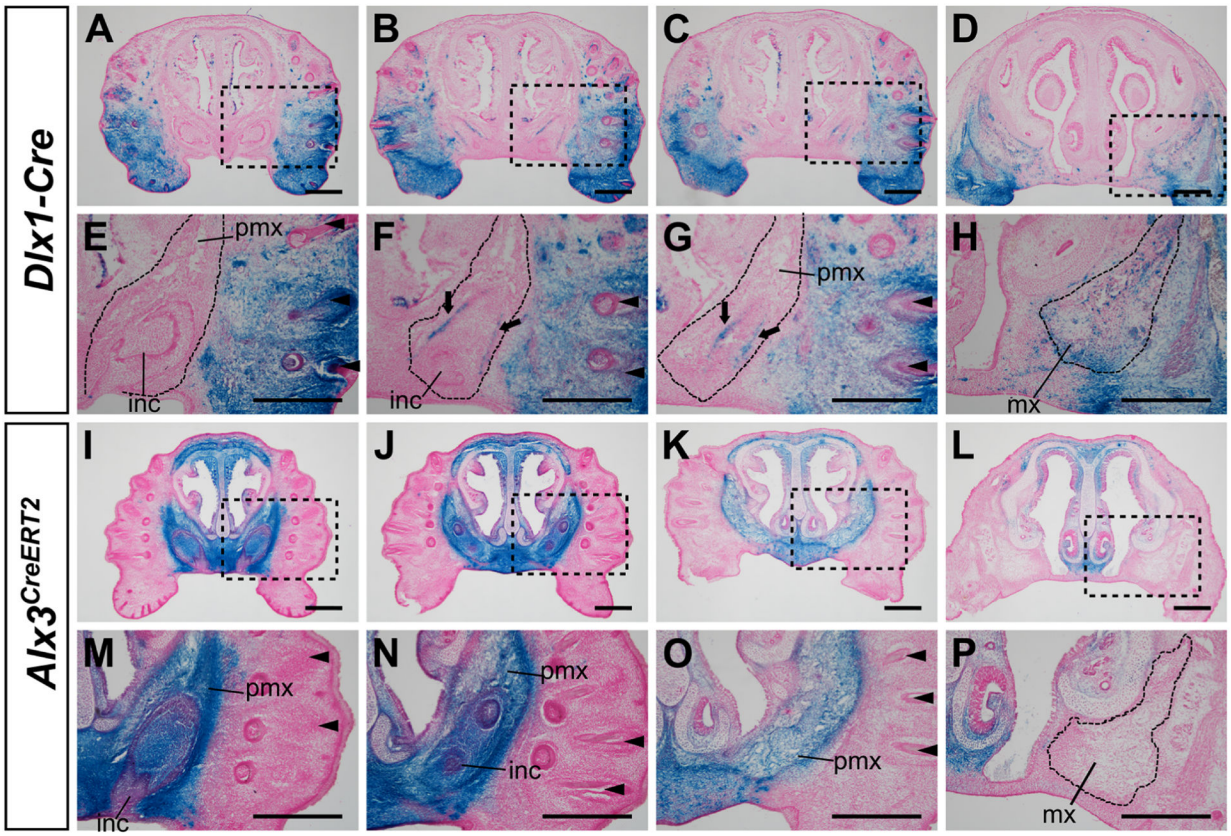

Figure 6. Comparative analyses of contributions of *Dlx1-Cre* and *Alx3*^{CreERT2} lineages in the developing upper jaw.

(A-D) Representative serial frontal sections of E15.5 *Dlx1-Cre;R26R*$^{lacz/+}$ embryo heads (n=4) showing patterns of β-gal lineage reporter (blue color). (E-H) Higher magnification views of the boxed regions in panels A-D, respectively. The premaxillary bone tissues in E-F and the maxillary bone tissue in H are marked by black dashed outline. Arrows in F and G point to the dental follicle cells by the *Dlx1-Cre* lineage reporter. (I-L) Representative serial frontal sections of E15.5 *Alx3*$^{CreERT2/+}$*;R26R*$^{lacz/+}$ embryo heads (n=4) showing patterns of β-gal lineage reporter (blue color). (M-P) Higher magnification views of the boxed regions in panels I-L, respectively. The premaxillary bone tissues in I-K and the maxillary bone tissue in L are marked by black dashed outlines. Arrowheads in E-G and M-O point to the vibrissae. Scale bars 500 μm. inc, incisor; mx, maxillary bone; pmx, premaxillary bone.

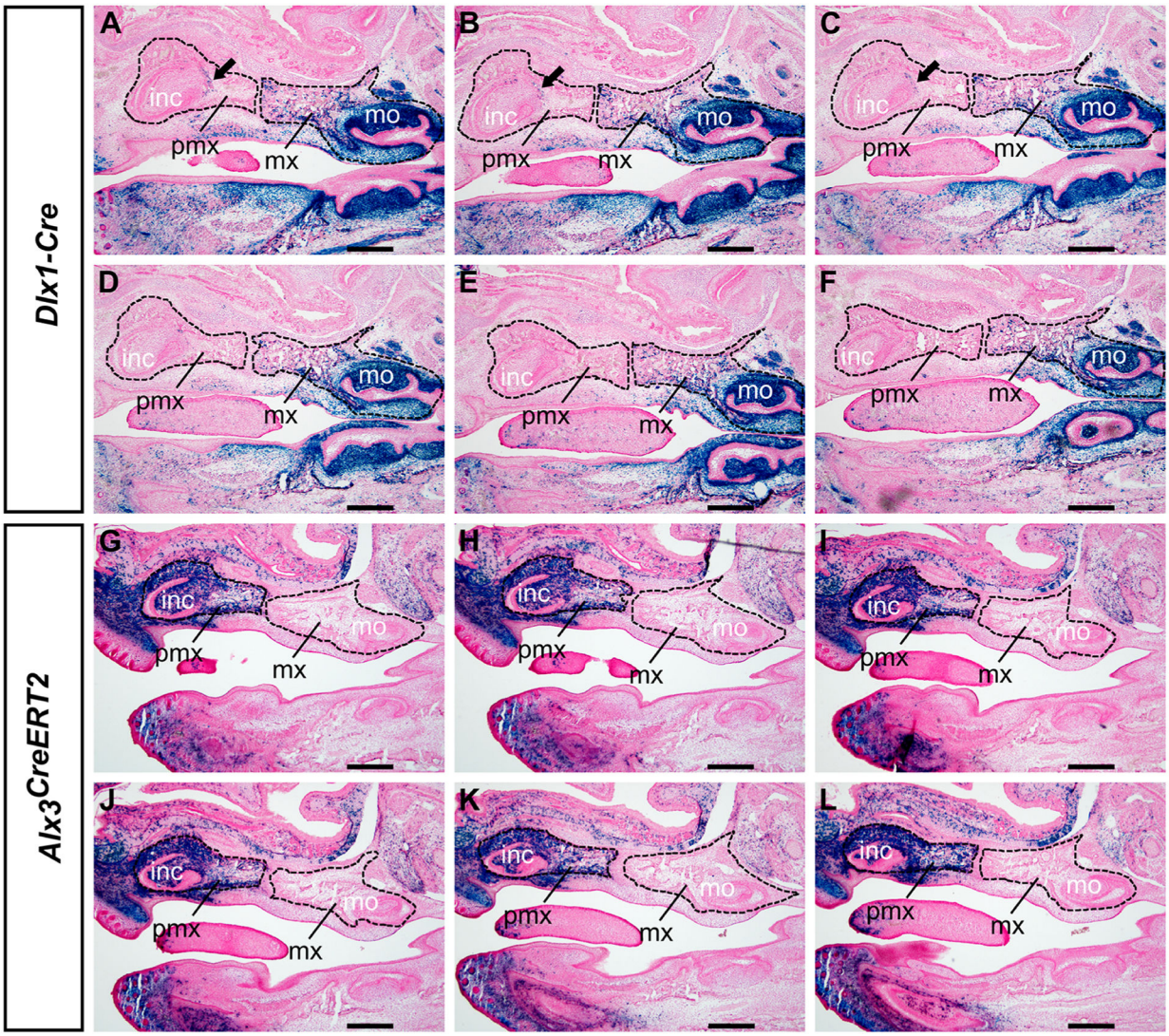

Figure 7. Comparative analyses of contributions of *Dlx1-Cre* and *Alx3*^{CreERT2} lineage cells to the premaxillary and maxillary bones.

(A-F) Representative serial parasagittal sections of E16.5 *Dlx1-Cre;R26R*$^{lacz/+}$ embryo heads (n=4) showing patterns of β-gal lineage reporter (blue color) at the premaxillary-maxillary regions from the buccal side to the lingual side. The premaxillary and the maxillary bone tissues are marked by black dashed outlines. Arrows in A-C point to the dental follicle cells labelled by the *Dlx1-Cre* lineage reporter. (G-L) Representative serial parasagittal sections of E16.5 *Alx3*$^{CreERT2/+}$*;R26R*$^{lacz/+}$ embryo heads (n=4) (following tamoxifen treatment at E9.5) showing patterns of β-gal lineage reporter (blue color) at the premaxillary-maxillary regions from the buccal side to the lingual side. inc, incisor; mo, first molar tooth germ; mx, maxillary bone; pmx, premaxillary bone.